Journal of Applied Mathematics and Physics, 2025, 13(12), 4548-4566
https://www.scirp.org/journal/jamp
ISSN Online: 2327-4379
ISSN Print: 2327-4352

Investigation of Tensoelectric and Dielectric Properties of Bi_2Te_2-Bi_2Sb_2 Solid Solution Films under Microwave Field Exposure

Nosirjon Khaydarovich Yuldashev, Dilkhumor Tolibjanovna Mamadieva, Rustamjon Uktamovich Siddikov, Khusanboy Mannopovich Sulaymonov

Department of Physic, Fergana State Technical University, Fergana, Uzbekistan
Email: uzferfizika@mail.ru

How to cite this paper: Yuldashev, N.Kh., Mamadieva, D.T., Siddikov, R.U. and Sulaymonov, Kh.M. (2025) Investigation of Tensoelectric and Dielectric Properties of Bi_2Te_2-Bi_2Sb_2 Solid Solution Films under Microwave Field Exposure. *Journal of Applied Mathematics and Physics*, **13**, 4548-4566.
https://doi.org/10.4236/jamp.2025.1312249

Received: November 8, 2025
Accepted: December 21, 2025
Published: December 24, 2025

Abstract

The article presents the results of a study of the tensoelectric and dielectric properties of polycrystalline films of the Bi_2Te_3-Bi_2Sb_3 solid solution in the microwave frequency range of the electromagnetic field with the aim of determining the mechanisms of influence of point and extended inhomogeneities on the operating parameters of strain gauges for the accumulation of fatigue damage. Some properties of the specific electrical conductivity, impedance, and permittivity of these films are examined as functions of temperature and uniaxial tensile strain. Experimentally observed optical and deformation effects in the studied films under exposure are qualitatively interpreted using the effective medium model. It has been shown that the microwave strain gauge coefficients under static tensile strain depend significantly on the time and temperature of film annealing in atmospheric air. At t_{ann} = 1 - 1.5 h and T_{ann} = 500 K, stable film parameters are achieved for Bi_2Te_3-Bi_2Sb_3. The observed film properties are due to changes in the microstructure and charge carrier concentration in the $(Bi_xSb_{1-x})_2Te_3$ films after heat treatment. This method of study can serve as a means of measuring charge carrier concentration in inhomogeneous semiconductor structures.

Keywords

Polycrystalline Film, Bi_2Te_3-Bi_2Sb_3, Specific Conductivity, Impedance, Permittivity, Microwave Field, Mechanical Deformation, Heat Treatment

1. Introduction

Solid solutions of bismuth and antimony chalcogenides are effective thermoelec-

tric [1]-[6] and tenso-electric [7] [8] materials. They are utilized not only for thermoelectric cooling and heating, the thermoelectric conversion of energy, and as topological insulators that efficiently block electromagnetic interference, but also for the development of sensors designed to detect the accumulation of fatigue damage. Currently, significant attention is directed toward identifying the regularities in the formation of the structure and phase composition of polycrystalline films based on the solid solution $(Bi_xSb_{1-x})_2Te_3$, as well as investigating their electrical conduction mechanisms and dielectric characteristics. Thus, in works [6]-[8], "metallic" and "semiconducting" types of conductivity depending on temperature have been observed. In our previous work [7], it was shown that the electrical conductivity of porous polycrystalline $(Bi_{0.3}Sb_{0.7})_2Te_3$ films grown by thermal vacuum evaporation at substrate temperatures $T_s \le 363$K sharply increases at a threshold frequency of the alternating voltage $\omega_0 \approx 10^5$ Hz, while the characteristic temperature is $T_s \approx 423$ K. After approximately $N \approx 10^5$ switching cycles, the resistivity reaches $\varepsilon = \pm 1 \times 10^{-3}$ rel. unit. It was established that the change in resistivity upon achieving the threshold angular frequency ω_0, determined by the nonuniformity of the films, increases by about 10^2 times.

In thin semiconductor polycrystalline films, as opposed to bulk crystals and conventional polycrystalline materials, a reduction in film thickness leads to pronounced modifications in their electrophysical behavior. This is primarily attributed to the significant contribution of surface and near-surface charge transport, which is influenced by adsorption processes, impurity diffusion, and the presence of surface electronic states. The impact of the interfacial transition layer between the film and the substrate, thickness inhomogeneities arising from the fabrication technique, as well as quantum size effects observed in ultrathin films, becomes increasingly evident as the dimensions decrease. Moreover, it is essential to account for factors such as the structural quality of the film, its porosity, the occurrence of multiphase inclusions, and the presence of both point and extended structural defects, all of which substantially affect the resulting physical properties. The purpose of this work is to investigate the tensometric and dielectric properties of polycrystalline films $(Bi_xSb_{1-x})_2Te_3$ in a microwave field in the actual temperature range of 280 - 480 K in order to identify the mechanisms of the influence of film inhomogeneity on the behavior of the samples under study. The properties of the specific electrical conductivity, impedance, and permittivity of these films were studied as functions of temperature and uniaxial tensile strain. The experimentally observed optical and deformation effects in the studied films under the action of a microwave field were qualitatively interpreted using the effective medium model.

2. Experimental Technique

Impedance is a parameter that characterizes the electrical response of polycrystalline films at a specified frequency of an alternating electromagnetic field ($Z = R + iR_{LC}$, where R, $R_{LC} = \omega L - (1/\omega C)$, represent the active and reactive components of resistance, $\omega = 2\pi\nu$ is the angular frequency, and L and C denote

the inductance and capacitance of the film, respectively. Therefore, the precise determination of impedance is essential for evaluating the tensometric properties of samples exposed to an alternating field. In particular, analyzing the impedance of structurally inhomogeneous films based on the solid solution $(Bi_xSb_{1-x})_2Te_3$ as a function of relative strain $\xi = \Delta\ell/\ell_0$ enables the determination of the complex tensosensitivity coefficient in the microwave frequency range:

$$K = K_R + iK_{LC}, \tag{1}$$

where

$$K_R = \frac{\Delta R}{R_0 \cdot \xi}, \quad K_{LC} = \frac{\Delta R_{LC}}{R_{LC}^0 \cdot \xi}, \tag{2}$$

are the tensosensitivity coefficients for the active and reactive resistances, $\Delta R = R(\xi) - R_0$, $R(\xi)$ and R_0 are the film's active resistance with and without deformation.

Polycrystalline films of the solid solution $(Bi_xSb_{1-x})_2Te_3$ with different values of x from 0 to 0,5 were obtained and investigated. The film samples with the composition $(Bi_{0.3}Sb_{0.7})_2Te_3$ exhibited the best tensometric parameters, due to their phase composition and microscopic structure in the bulk and at the boundaries of crystalline grains. The choice of this particular composition is also due to the fact that the literature data [7]-[10] indicate that, in the system of solid solutions $(Bi_xSb_{1-x})_2Te_3$, the composition $(Bi_{0.3}Sb_{0.7})_2Te_3$ possesses the highest tensosensitivity. Polycrystalline films with a thickness of 3 - 4 μm and dimensions of 5 × 30 mm on a polyamide substrate were fabricated by thermal evaporation in vacuum at $P \cdot 10^{-2}$ Pa, at a substrate temperature of $T_n = 363$ K and a deposition rate of $W \approx 200$ Å/s [9] [10].

The polycrystalline films under investigation were placed into a measurement cell containing a waveguide section equipped with a heating system, which enabled temperature control within the range of 77 - 480 K and provided microwave field frequencies from 10^8 to 10^{11} Hz. Impedance spectroscopy was performed using a measurement procedure analogous to that described in [11] [12].

The specific electrical conductivity was determined as,

$$\sigma = \frac{\ell}{b \cdot d}\frac{I}{V_\sigma}, \tag{3}$$

where ℓ, b, d, length, width, and thickness of the sample, respectively; I is the current through the sample; V_σ—voltage drop between the electrodes used to measure the conductivity.

Deformation was induced by bending a cantilever plate of a standard equal-resistance deformation device fabricated from a titanium alloy. The film samples, attached to the plate using a specialized adhesive, were subjected to uniaxial tensile strain through the bending of the substrate. The magnitude of the relative strain ξ was calculated using the well-known expression given in [13]:

$$\xi = \frac{4d}{\ell^2} \cdot y, \tag{4}$$

where y—deflection of the free end of the plate at the point of force application. The deformation values varied in the range from от $\xi = 0$ to $\xi = +6 \times 10^{-3}$ rel. unit. conventional units. The study of dielectric permittivity under the action of mechanical deformation was carried out mainly at a fixed frequency of $\omega = 5.1 \times 10^{10}$ Hz.

Along with significant advances in the technology of fabrication and investigation of the properties of thin-film elements based on narrow-bandgap semiconductor compounds and their solid solutions, a number of their drawbacks have also been identified. These include insufficient stability and low sensitivity of structural properties. Eliminating these drawbacks requires a deeper study of the physical processes occurring in inhomogeneous semiconductor films.

Films of the solid solution $(Bi_xSb_{1-x})_2Te_3$ can be considered as consisting of two components, Bi_2Te_3 and Bi_2Sb_3, with an excess of one of these components (for $x \neq 0.5$). Low values of the carrier concentration N and Hall mobility $\mu_x = R_x\sigma$, as well as the specific conductivity σ, indicate that the film material represents a strongly inhomogeneous medium. A characteristic feature of such inhomogeneous media is the dependence of the effective complex dielectric permittivity (ε_{eff}^*) and specific electrical conductivity (σ_{eff}^*) on the frequency of the alternating field. Additionally, the values of ε_{eff}^* and σ_{eff}^* are functions of the relative volume fraction, shape, dielectric permittivity, and electrical conductivity of each component constituting the inhomogeneous medium.

3. Theory

Dielectric permittivity and electrical conductivity of heterogeneous films in the microwave frequency range. Based on the effective medium approximation [14]-[18], the impact of the volume proportions of constituents and their geometrical arrangement on the real ($\mathrm{Re}\,\varepsilon_{eff}^*$), the minimum imaginary ($\mathrm{Im}\,\varepsilon_{eff}^*$) part of ε_{eff}^* the permittivity, and the real ($\mathrm{Re}\,\sigma_{eff}^*$) component of the conductivity σ_{eff}^* of bismuth-antimony telluride films with disrupted stoichiometry in the microwave frequency domain was examined. The effective characteristics of the film were evaluated using the self-consistent local field approach. According to this concept [17], it is feasible to determine the field distribution around a single element of a multiphase medium selected as its representative. In this scenario, it is assumed that the chosen element is embedded in an effective medium defined by the condition of null total perturbation field, which is caused by components independent of velocity in the static regime.

For two-component heterogeneous media, the electric field averaged over the volume of the medium E is equal to:

$$E = \frac{1}{V}\int_V E\mathrm{d}V = \frac{1}{V}\sum_{\kappa}\int_{V_\kappa} E_\kappa\,\mathrm{d}V_\kappa\ . \tag{5}$$

For an inhomogeneous medium placed into a homogeneous field E, the field E_κ is homogeneous but different for each component. Therefore, expression (5) can

be represented as:

$$E = \sum_{\kappa} \theta_{\kappa} E_{\kappa} . \tag{6}$$

The field E_{κ} is related to the homogeneous field of the medium by the following dependence:

$$E_{\kappa} = \frac{\varepsilon_{eff}^{*}}{\beta_{\kappa}\varepsilon_{\kappa}^{*} + (1-\beta_{\kappa})\varepsilon_{eff}^{*}} \cdot E_{aver} . \tag{7}$$

Note that in (5)-(7), V is the volume of the film, $\theta_{\kappa} = V_{\kappa}/V$ —volume fraction of the component, ε_{κ}^{*} —complex dielectric permittivity, and β_{κ} —depolarization factor of each component. Substituting (7) into (6) and taking into account that the components of the medium have the same geometrical shape $(\beta_2 = \beta_1 = \beta)$, we obtain:

$$\theta_1 \frac{\varepsilon_{eff}^{*}}{\beta_1\varepsilon_1^{*} + (1-\beta)\varepsilon_{eff}^{*}} + \theta_2 \frac{\varepsilon_{eff}^{*}}{\beta_2\varepsilon_2^{*} + (1-\beta)\varepsilon_{eff}^{*}} = 1 . \tag{8}$$

In (8), assuming $\beta = 1/3$ (spherical inclusions) and solving with respect to ε_{eff}^{*}, we obtain:

$$\varepsilon_{eff}^{*} = A^{*} \pm \sqrt{A^{*2} + B^{*2}} , \tag{9}$$

where

$$A^{*} = \left[2\left(\varepsilon_1^{*} + \varepsilon_2^{*}\right) - 3\left(\theta_1\varepsilon_2^{*} + \theta_2\varepsilon_1^{*}\right)\right]/4 , \tag{10}$$

$$B^{*} = \varepsilon_1^{*}\varepsilon_2^{*}/2 , \quad \varepsilon_1^{*} = \varepsilon_1 + i4\pi\sigma_1/\omega , \quad \varepsilon_2^{*} = \varepsilon_2 + i4\pi\sigma_2/\omega , \tag{11}$$

ε_1 и ε_2 —are the real dielectric permittivity parts of Bi_2Te_3 and Bi_2Sb_3, while σ_1 and σ_2 —are the conductivities of these components in an alternating field, ω —field frequency.

In an alternating field, the complex electrical conductivity can be represented as:

$$\sigma^{*} = \sigma_0 \frac{1 - i\omega\tau}{1 + \omega^2\tau^2} , \tag{12}$$

where $\sigma_0 = N\dfrac{e^2\tau}{m^{*}}$ —DC electrical conductivity, N—concentration of charge carriers, e—electron charge, τ —relaxation time, m^{*} —effective mass of free carriers. Taking into account the relation $\varepsilon^{*} = (n - i\kappa)^2$ (where n—refractive index, κ—absorption coefficient) and substituting (12) into (11), we obtain respectively

$$\varepsilon_1^{*} = \varepsilon_1 - 4\pi\sigma_0'\tau_1\left(1 + \omega^2\tau_1^2\right)^{-1} + i4\pi\sigma_0''\left[\omega\left(1 + \omega^2\tau_1^2\right)\right]^{-1} ,$$

$$\varepsilon_2^{*} = \varepsilon_2 - 4\pi\sigma_0'\tau_2\left(1 + \omega^2\tau_2^2\right)^{-1} + i4\pi\sigma_0''\left[\omega\left(1 + \omega^2\tau_2^2\right)\right]^{-1} .$$

Separating the real and imaginary parts in the latter equations, we obtain:

$$\operatorname{Re}\varepsilon_1^{*} = n_1^2 - \kappa_1^2 = \varepsilon_1 - 4\pi\omega^{-1}\operatorname{Im}\sigma_1 , \tag{13}$$

$$\operatorname{Im}\varepsilon_1^* = 2n_1\kappa = \frac{4\pi \operatorname{Re}\sigma_1}{\omega}, \tag{14}$$

$$\operatorname{Re}\varepsilon_2^* = \varepsilon_2 - \frac{4\pi}{\omega}\operatorname{Im}\sigma_2, \tag{15}$$

$$\operatorname{Im}\varepsilon_2^* = 2n_2\kappa_2 = \frac{4\pi \operatorname{Re}\sigma_2}{\omega}. \tag{16}$$

Substituting them into (12) and (11), we obtain the expressions for calculating the real and imaginary parts of A^* и B^*

$$\begin{aligned}\operatorname{Re}A^* = &\left[2\left(\varepsilon_1+\varepsilon_2\right)-3\left(\theta_1\varepsilon_2+\theta_2\varepsilon_1\right)\right]/4\\ &+\frac{\pi}{\omega}\left[3\left(\theta_1\operatorname{Im}\sigma_2+\theta_2\operatorname{Im}\sigma_1\right)-2\left(\operatorname{Im}\sigma_1+\operatorname{Im}\sigma_2\right)\right],\end{aligned} \tag{17}$$

$$\operatorname{Im}A^* = \frac{2\pi}{\omega}\operatorname{Re}\left(\sigma_1+\sigma_2\right)-\frac{3\pi}{\omega}\left(\theta_1\operatorname{Re}\sigma_2+\theta_2\operatorname{Re}\sigma_1\right), \tag{18}$$

$$\operatorname{Re}B^* = \frac{\varepsilon_1\varepsilon_2}{2}-\frac{2\pi}{\omega}\left(\varepsilon_1\operatorname{Im}\sigma_2+\varepsilon_2\operatorname{Im}\sigma_1\right)+\frac{8\pi^2}{\omega^2}\left(\operatorname{Im}\sigma_1\operatorname{Im}\sigma_2-\operatorname{Re}\sigma_1\operatorname{Re}\sigma_2\right), \tag{19}$$

$$\operatorname{Im}B^* = \frac{2\pi}{\omega}\left(\varepsilon_1\operatorname{Re}\sigma_2+\varepsilon_2\operatorname{Re}\sigma_1\right)-\frac{8\pi^2}{\omega^2}\left(\operatorname{Im}\sigma_1\operatorname{Re}\sigma_2+\operatorname{Re}\sigma_1\operatorname{Im}\sigma_2\right). \tag{20}$$

We introduce the notation $\sqrt{A^{*2}+B^{*2}} = \sqrt{a+i\text{в}}$.

Hence

$$a = \operatorname{Re}A^2 - \operatorname{Im}A^2 + \operatorname{Re}B, \tag{21}$$

$$\text{в} = 2\operatorname{Re}A\operatorname{Im}A - \operatorname{Im}B, \tag{22}$$

from the relation $\sqrt{a+i\text{в}} = c+id$ we find

$$c = \sqrt{\frac{a}{2}\pm\sqrt{\frac{a^2}{4}+\frac{\text{в}^2}{4}}}, \tag{23}$$

where $d = e/(2c)$.

Taking the above into account, it is not difficult to determine the real and imaginary parts of the effective dielectric permittivity, respectively

$$\operatorname{Re}\varepsilon_{eff} = \operatorname{Re}A + c, \tag{24}$$

$$\operatorname{Im}\varepsilon_{eff} = \operatorname{Im}A + d. \tag{25}$$

These results allow the real part of the effective conductivity of the films to be written in the form

$$\operatorname{Re}\sigma_{eff} = \frac{\omega}{4\pi}\cdot\operatorname{Im}\varepsilon_{eff}.. \tag{26}$$

Using the relation for the absorption coefficient $\alpha = 2\omega\kappa/c$ (c—speed of light), we obtain the real part of the conductivity of the individual film components, respectively

$$\operatorname{Re}\sigma_1 = \frac{\alpha_1 n_1 c}{4\pi} \text{ и } \operatorname{Re}\sigma_2 = \frac{\alpha_2 n_2 c}{4\pi}. \tag{27}$$

The imaginary part can be determined from relations (13) and (15). All param-

eters $\varepsilon_{eff}, \sigma_{eff}$ can be considered determined if the values n, κ and d are known. For polycrystalline films, these coefficients are obtained from experimental data.

For the theoretical calculation of the absorption coefficient α, the relation connecting $\alpha(\omega)$ and $\sigma(\omega)$ was used [23]

$$\alpha(\omega) = \frac{4\pi}{c\sqrt{\varepsilon_1}}\sigma(\omega). \tag{28}$$

Here $\varepsilon_1, \sigma(\omega)$—real part of the dielectric permittivity and the specific conductivity, respectively. It is known that $\operatorname{Im}\varepsilon = \frac{4\pi \operatorname{Re}\sigma}{\omega}$ therefore, for the absorption coefficient we obtain

$$\alpha(\omega) = \frac{\omega \operatorname{Im}\varepsilon_{eff}}{c\sqrt{\operatorname{Re}\varepsilon_{eff}}}. \tag{29}$$

4. Experimental Results and Their Discussion

The frequency dependences of $\operatorname{Im}\varepsilon_{eff}$ for the $(Bi_xSb_{1-x})_2Te_3$ films with an excess of antimony telluride and with an excess of bismuth telluride were obtained on the basis of formula (25) and are presented in **Figure 1** and **Figure 2**. Numerical calculations were performed using the following parameter values: $\sigma_0' = 5.7(\Omega\cdot\text{cm})^{-1}$, $\varepsilon_1 = 55$; $\sigma_0'' = 3.25(\Omega\cdot\text{cm})^{-1}$, $\varepsilon_2 = 45$. The graphical dependences $\operatorname{Re}\varepsilon_{eff}$ and $\operatorname{Re}\sigma_{eff}$ ω, obtained according to formulas (24) and (25), are similar to the behavior of $\operatorname{Im}\varepsilon_{eff}$. For all investigated films, the dependence on θ exhibits a shift both in the energy scale and in intensity. The values $\operatorname{Im}\varepsilon_{eff}$, $\operatorname{Re}\varepsilon_{eff}$ and $\operatorname{Re}\sigma_{eff}$ in the frequency region of intrinsic absorption $\hbar\omega \approx E_g$ (where, $E_g = 0.13$ eV for Bi_2Te_3 and $E_g = 0.21$ eV for Sb_2Te_3 at $T \approx 77$ K [19] [20]) reach their maximum

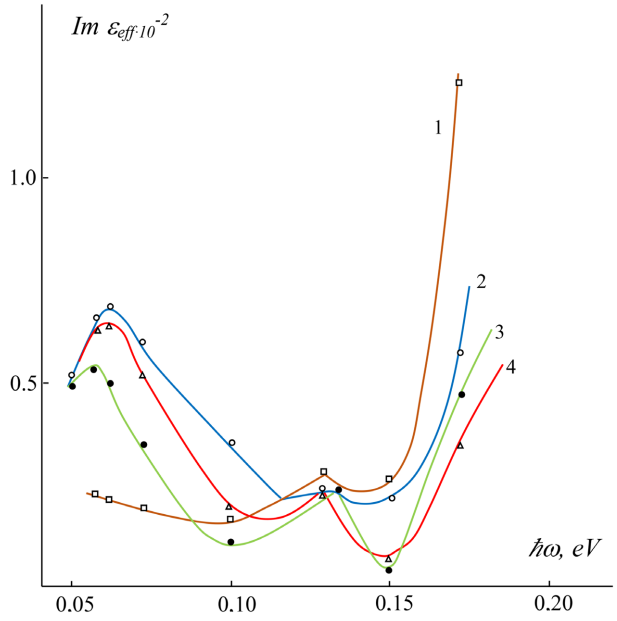

Figure 1. Spectrum of Im ε_{eff} for $(Bi_xSb_{1-x})_2Te_3$ films with an excess of antimony telluride in mass percentages: 1—0.8%; 2—1.8%; 3—2.8%; 4—3.8%.

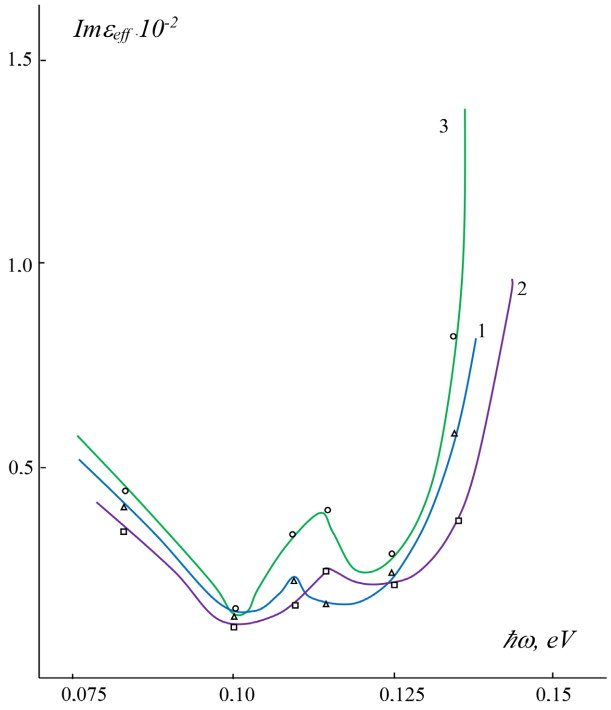

Figure 2. Spectrum of Im ε_{eff} for $(Bi_xSb_{1-x})_2Te_3$ films with an excess of bismuth telluride in mass percentages. 1—0.2%; 2—1.2%; 3—2.2%.

values ($\mathrm{Re}\,\varepsilon_{eff} > \varepsilon_1 > \varepsilon_2$,) ($\mathrm{Re}\,\sigma_{eff} > \sigma_0' > \sigma_0''$). In this case, the entire quantum energy of light is spent on transferring electrons from the valence band to the conduction band, which determines the imaginary part of the effective dielectric permittivity of the films.

The dependence of $\mathrm{Im}\,\varepsilon_{eff}$ and $\mathrm{Re}\,\varepsilon_{eff}$ on the composition of the films in the microwave frequency range, shown in **Figure 3**, was also investigated by the authors of work [19]. The results can be interpreted as follows. Under the action of an alternating field, free charge carriers are displaced over microscopic distances that exceed the conducting region of the sample. As a result, each conducting phase region becomes an electric dipole. Therefore, the sample becomes polarized. At certain threshold frequencies $\hbar\omega < E_g$ (in **Figure 1**, $\hbar\omega_1 \approx 0.056$ eV , $\hbar\omega_2 \approx 0.13$ eV and in **Figure 2**, $\hbar\omega_1 \approx 0.07$ eV , $\hbar\omega_2 \approx 0.115$ eV), all regions of the sample have enough time to fully polarize, which leads to an increase in both $\mathrm{Im}\,\varepsilon_{eff}$ and $\mathrm{Re}\,\varepsilon_{eff}$.

A relatively large value and growth of $\mathrm{Re}\,\varepsilon_{eff}$ with an increasing fraction of antimony telluride in the film composition is apparently associated with changes in the depolarization factor due to the crystalline sublattices of Bi_2Te_3 and Sb_2Te_3. However, with increasing bismuth telluride content, $\mathrm{Re}\,\varepsilon_{eff}$ decreases (curve 2′ in **Figure 3**), while $\mathrm{Im}\,\varepsilon_{eff}$ increases (curve 2). This is evidently related to the formation of metallic interlayers. As the calculations show, the dispersion of $\mathrm{Im}\,\varepsilon_{eff}$, $\mathrm{Re}\,\varepsilon_{eff}$ values is minimal for spherical inclusions, and maximal for inclusions in the form of an elongated ellipsoid. At high frequencies $\hbar\omega > E_g$ within a short time the electron system does not have enough time to polarize

(due to small values of Maxwell relaxation time), which leads to reduced effective dielectric permittivity values of the films. As experiments show, $\mathrm{Re}\sigma_{eff}$ for $(Bi_xSb_{1-x})_2Te_3$ films exceeds the corresponding values for the individual Bi_2Te_3 and Sb_2Te_3. This is apparently associated with the parallel connections of crystallites in the films.

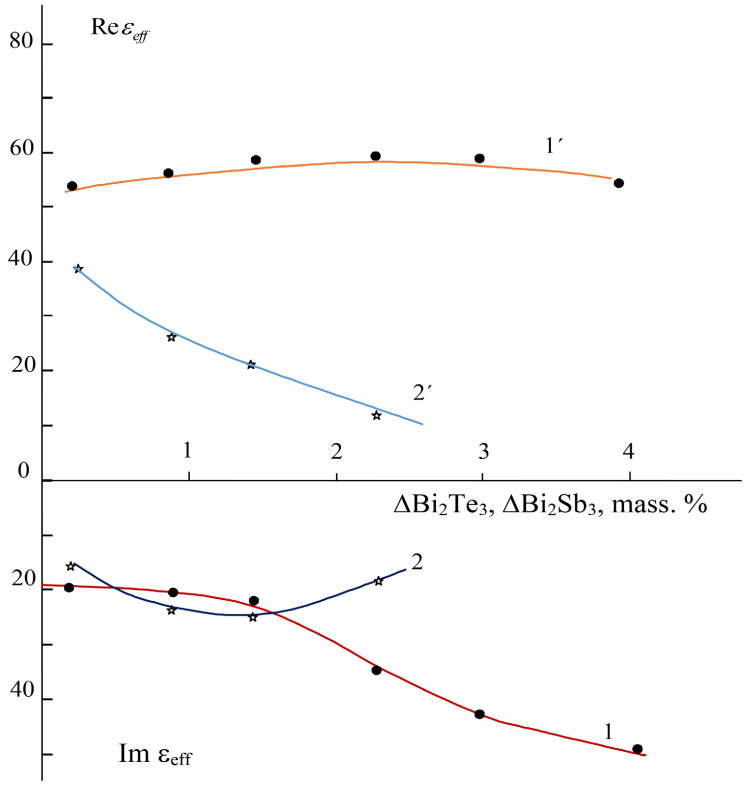

Figure 3. Dependence of $\mathrm{Im}\varepsilon_{eff}$, $\mathrm{Re}\varepsilon_{eff}$ on the composition of the films $(Bi_xSb_{1-x})_2Te_3$: 1, 1'—with an excess of antimony telluride; 2, 2'—with an excess of bismuth telluride.

In **Figure 4**, the experimental (curves 1, 3 with points) and theoretical (2, 4, calculated using formula (29)) spectra of the absorption coefficient $\alpha(\omega)$ for samples with an excess of antimony telluride of 1.8 mass.% (curves 1, 2) and 3.8 mass.% (curves 3, 4) are shown. As seen from the figure, the theoretical curves correspond well to the experimental ones, although the theoretical values in the frequency range $\hbar\omega < E_g$ are slightly lower than the experimental ones. However, when $\hbar\omega > E_g$, the reverse situation can occur. This correspondence is observed for all samples $(Bi_xSb_{1-x})_2Te_3$. Thus, the superstoichiometric additions of Bi_2Te_3 and Sb_2Te_3 in the solid solution range contribute to the formation of a wide concentration range of electrically active impurities. This promotes the growth of the film parameters $\varepsilon, \sigma, \alpha$. Moreover, the excess of these superstoichiometric impurities leads to the formation of a separate phase, the distribution of which can be nonuniform throughout the entire volume of the film, significantly affecting the polarization and, consequently, ε_{eff}. All of these factors, in combination, contribute to the increase of α.

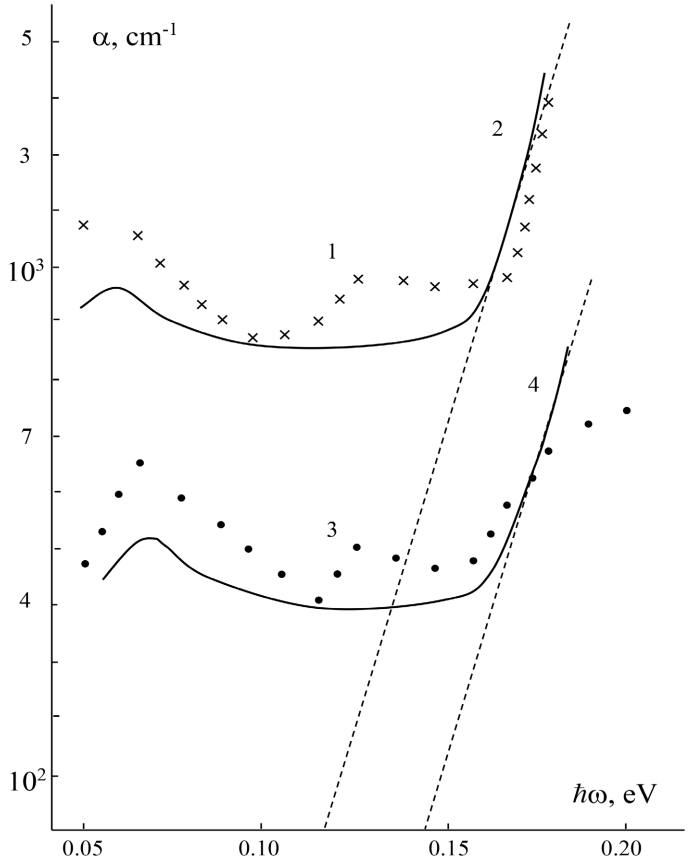

Figure 4. Absorption spectra of $(Bi_xSb_{1-x})_2Te_3$ films with an excess of antimony telluride: 1.8 mass.% (1, 2) and 3.8 mass.% (3, 4); 1,3—experiment; 2,4—theory.

The dependence of the conductivity of $(Bi_{0.3}Sb_{0.7})_2Te_3$ films on temperature is shown in **Figure 5**. As depicted in the figure, the real part of the electrical conductivity exhibits an increasing trend with rising temperature. Conversely, the imaginary part of the conductivity decreases progressively as the temperature increases, up to approximately 350 K. Within the investigated temperature range, the electrical conductivity demonstrates a relatively weak temperature dependence. It is noteworthy that the real component of conductivity determined using the continuous wave (CW) method significantly differs from the conductivity values obtained via the direct current (DC) measurement technique. This divergence can be ascribed to the fundamentally different measurement principles and frequency regimes inherent to each method. Additionally, microstructural characteristics of the films, such as the presence of defects, grain boundaries, and stoichiometric deviations, may further influence the observed discrepancies in conductivity values. Naturally, the conductivity of polycrystalline materials, such as $(Bi_{0.3}Sb_{0.7})_2Te_3$, measured by the CW method, is mainly determined by the electronic and structural inhomogeneities of the films. A comparison of the values of conductivity measured by the CW method and the DC method confirms the presence of these inhomogeneities in the studied samples. Polycrystalline $(Bi_{0.3}Sb_{0.7})_2Te_3$ films represent a non-uniform system consisting of individual crystalline regions

with different local conductivities. These heterogeneous systems exhibit high dielectric permittivity, the measurement of which allows for the calculation of the effective dielectric parameters of the components. The literature also discusses the issue of the structure of the microcrystals in films at high frequencies. However, this idea was not verified in studies involving the tensile strength of polycrystalline films $(Bi_xSb_{1-x})_2Te_3$ in the microwave frequency range.

It turned out that the CW method has several advantages in measuring certain quantities compared to measurements in the DC mode. Some bulk properties of the semiconductor have a number of interesting features related to the fact that the period associated with them is relatively short. The CW method has a frequency order of charge carrier collisions. CW measurements provide the opportunity to obtain additional information about their properties, which cannot be determined in DC measurements. This allows for the determination of the real and imaginary parts of the impedance, using which we can judge their contribution to the dielectric permittivity of the films.

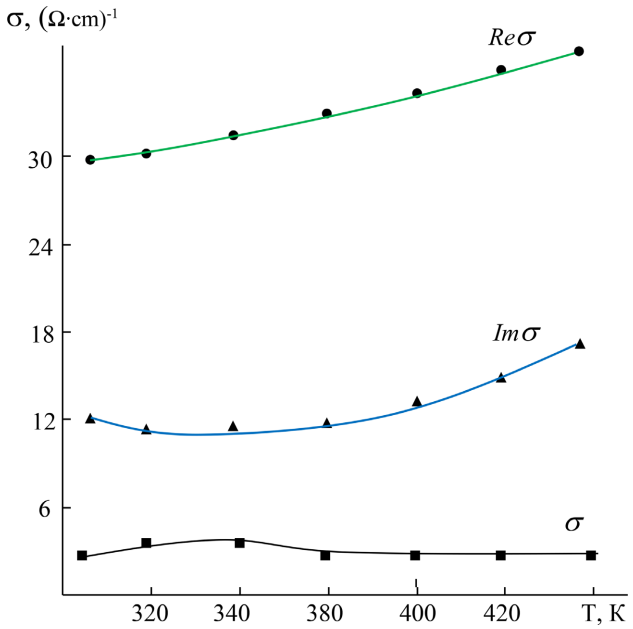

Figure 5. Dependence of the specific electrical conductivity of $(Bi_{0.3}Sb_{0.7})_2Te_3$ films on temperature.

Figure 6 illustrates the relationship between the real component of the impedance of polycrystalline $(Bi_{0.3}Sb_{0.7})_2Te_3$ films and temperature at varying degrees of relative strain. It is observed that with increasing relative strain and temperature, the impedance of the films initially rises and subsequently declines more rapidly, particularly at lower strain levels (the real part of the impedance of unstrained films exhibits a weak temperature dependence).

The temperature dependence of the imaginary part of the electrical conductivity of n-type $(Bi_{0.3}Sb_{0.7})_2Te_3$ thin films under different levels of uniaxial deformation, plotted in the coordinates $\ell n\,\mathrm{Im}\,\sigma - 1/T$, is shown in **Figure 7**. The re-

sults reveal that the imaginary component of the conductivity of $(Bi_{0.3}Sb_{0.7})_2Te_3$ films decreases consistently with increasing temperature and the magnitude of uniaxial strain. At temperatures above 360 K, this trend no longer holds: the imaginary part of the electrical conductivity initially shows a slight increase with temperature before subsequently declining, indicating a change in the dominant transport processes at elevated temperatures.

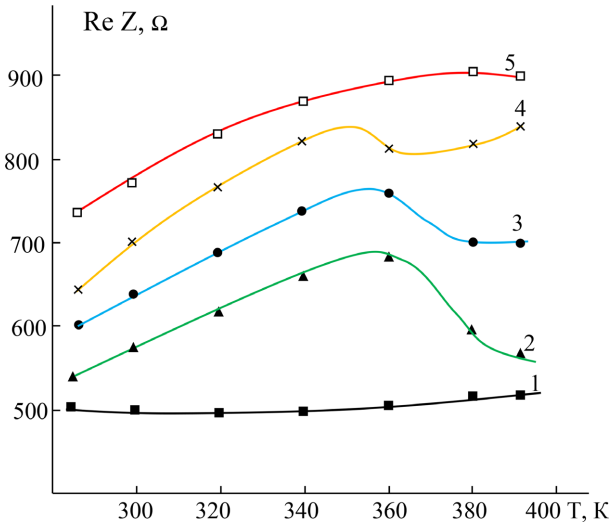

Figure 6. Dependence of the real part of the impedance of $Bi_{0.3}Sb_{0.7})_2Te_3$ on temperature at various levels of tensile deformation $\xi \cdot 10^3$: 1—0, 2—1.12; 3—2.27; 4—3.4; 5—4.52.

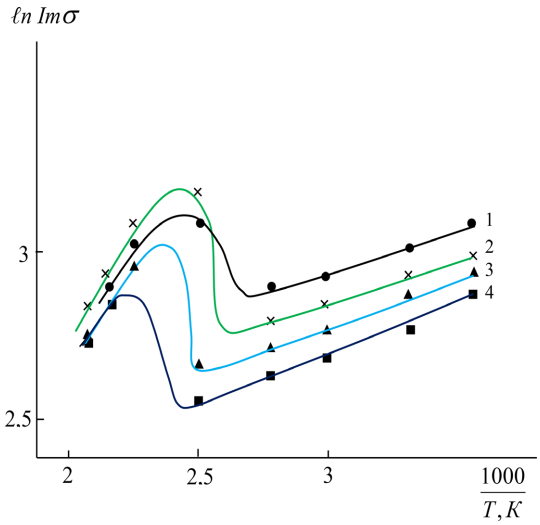

Figure 7. Dependence of $\ell n\ Im\sigma$ on $1/T$ for $(Bi_{0.3}Sb_{0.7})_2Te_3$ films at various levels of relative deformation $\xi \cdot 10^3$: 1—0, 2—1.4; 3—2.8; 4—4.2.

The sensitivity of the impedance of $(Bi_{0.3}Sb_{0.7})_2Te_3$ films in the microwave range to external mechanical deformations makes it possible to determine the piezoresistive properties of these films. Studies of the piezoelectric effect in polycrystalline films by the MW method make it possible to identify the mechanism of high piezoresistivity. Analyzing the experimental data, it can be noted that abnormally

high piezoresistivity is not observed in all polycrystalline film samples.

In the simplest scenario, thin-film specimens utilized as strain sensors should comprise two phases whose electrical conductivities differ by specific ratios. The effective conductivity of a heterogeneous medium depends on the conductivities of its constituents and their volumetric proportions. As the volume fraction of the secondary phase increases, the overall electrical conductivity varies following a defined relationship (from σ_1 to σ_2). If a gradual variation in effective conductivity with increasing volume fraction of the secondary phase is observed, such specimens will demonstrate piezoelectric (strain-sensitive) behavior, albeit with relatively low sensitivity. Conversely, if a sudden change in effective conductivity occurs within a certain range of the secondary-phase volume fraction, the piezoresistive sensitivity of these specimens may attain its peak value. Within this narrow interval of the secondary-phase volume fraction, fluctuations in the polarizability of crystallites under the influence of uniaxial tensile strain reach their maximum magnitude.

The non-contact microwave method serves as a powerful instrument for investigating the complex piezoresistive sensitivity of $(Bi_xSb_{1-x})_2Te_3$, thin films that have undergone thermal annealing in air. Therefore, the regularities of the variation of the real and imaginary parts of the piezoresistive sensitivity of $(Bi_{0.3}Sb_{0.7})_2Te_3$ films were investigated under different temperatures and annealing durations.

Figure 8 illustrates the relationship between *ReK* and annealing duration at various levels of relative strain, with the annealing temperature held constant at t_{refl} = 500 K. It is apparent that as the annealing duration and relative tensile strain increase, *ReK* decreases. However, within the time interval from 2.5 to 4.5 hours, the linear correlation between *ReK* and annealing time is disrupted.

In Figure 9, shows the dependence of I_mK on annealing time at various levels

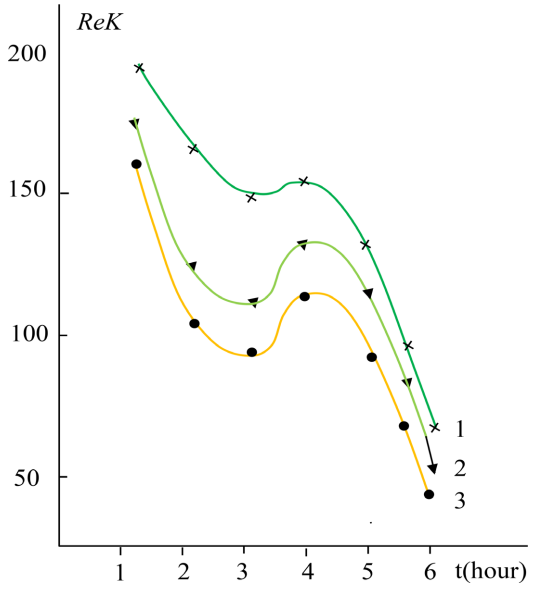

Figure 8. Dependence of the real part of the piezoresistive coefficient of $(Bi_{0.3}Sb_{0.7})_2Te_3$ on annealing time at different levels of relative deformation $\xi 10^3$: 1—3.3; 2—4.5; 3—5.6.

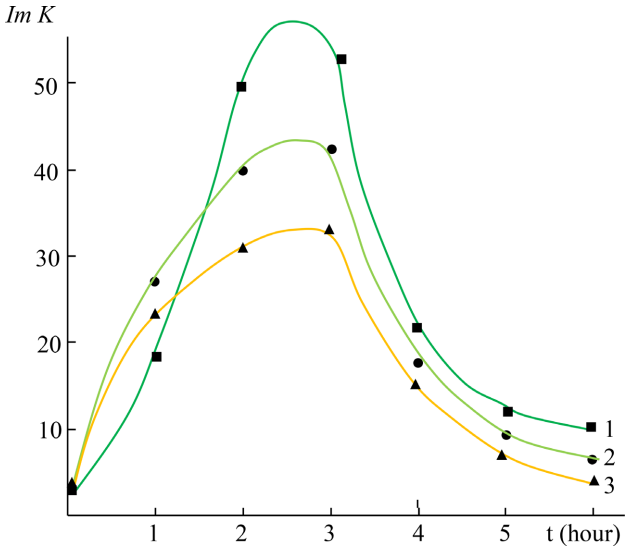

Figure 9. Dependence of the imaginary part of the piezoresistive coefficient of $(Bi_{0.3}Sb_{0.7})_2Te_3$ on annealing time at various levels of relative deformation $\xi \cdot 10^3$: 1—1.12; 2—2.27; 3—3.30.

of relative deformation. It can be observed that with increasing annealing time, I_mK increases, and after reaching a maximum, decreases exponentially. The value of I_mK remains positive throughout the entire annealing range. It is assumed that the change in the piezoresistive coefficient in the microwave range during air annealing is due to the change in charge carrier concentration in $(Bi_xSb_{1-x})_2Te_3$ films. The microwave method makes it possible to register variations in charge carrier concentration.

Deformation phenomena in polycrystalline films under the influence of microwave fields can be analyzed based on the theory of the effective medium [14]-[18]. During thermal treatment of the films in air, the concentration of charge carriers changes in the interfacial regions of the crystallites. When the crystallite size becomes comparable to the diffusion length of oxygen, the medium primarily contains a second phase. In such films, one should not expect anomalous piezoresistive effects. If no heterogeneities are present in the films, i.e., if they are perfectly homogeneous, then the piezoresistive sensitivity of such samples should be minimal.

The increase in the piezoresistive coefficient is caused by fluctuations in the current density in the spatial coordinates of the films. This effect is associated with the presence of thermally induced inhomogeneities, which generate surface conductivity in the crystallites that differs substantially from bulk conductivity. The surface conductivity is a function of the oxygen diffusion length. If the volume of these interfacial layers equals that of the main material, then the effective complex conductivity changes rapidly, and at this point, fluctuations in current density reach their maximum. The observed maximum in the imaginary part of the piezoresistive coefficient with increasing annealing time is consistent with the explanations given above.

Note that the dielectric properties of bismuth tellurides are characterized by

large static and optical dielectric constants ε_s, ε_∞; as well as low frequencies of transverse optical phonons. The dielectric permittivity of Bi_2Te_3 films has a high value of $\varepsilon_\infty \approx 45$ (for Sb_2Te_3 $\varepsilon_\infty \approx 55$) and in the temperature range from 193 to 400 K weakly depends on temperature [20] [21].

In **Figure 10**, the dependence of $\ell n\ \varepsilon_s$ on the inverse temperature at various levels of deformation is presented. It is evident that the dielectric permittivity of the $(Bi_{0.3}Sb_{0.7})_2Te_3$ films exhibits an activation-type behavior. As the temperature increases up to 400 K, the dielectric permittivity rises and then decreases, i.e., a broad maximum is observed. A similar trend is also found when studying the imaginary part of the dielectric permittivity of $(Bi_{0.3}Sb_{0.7})_2Te_3$ films versus the inverse temperature at different tensile deformation levels in the microwave frequency range. The absolute value of the imaginary component is approximately one order of magnitude lower than the real component of the dielectric permittivity. Experimental results demonstrate that the real part of the dielectric permittivity for polycrystalline $(Bi_{0.3}Sb_{0.7})_2Te_3$ films attains a value of 5.3×10^4, whereas the imaginary part reaches 7.1×10^3 units (see **Figure 11**). We attribute these observations to the interaction of the film with atmospheric oxygen under the combined effects of thermal exposure and mechanical deformation. In particular, localized electronic states generated at the grain boundaries of the crystals contribute significantly to these phenomena.

Moreover, the evolution of local heterogeneities and the incorporation of the secondary phase with increasing temperature induce substantial modifications in the dielectric properties of the polycrystalline $(Bi_{0.3}Sb_{0.7})_2Te_3$ films. Such changes reflect the complex interplay between microstructural dynamics and external stimuli, influencing both polarizability and charge transport mechanisms within

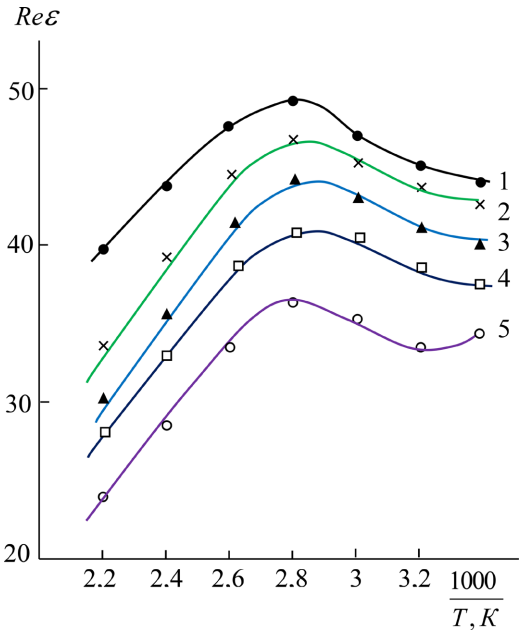

Figure 10. Dependence of the real part of the dielectric permittivity of $(Bi_{0.3}Sb_{0.7})_2Te_3$ on temperature at various levels of deformation $\xi 10^3$: 1—0; 2—0.68; 3—1.36; 4—2.04; 5—3.4.

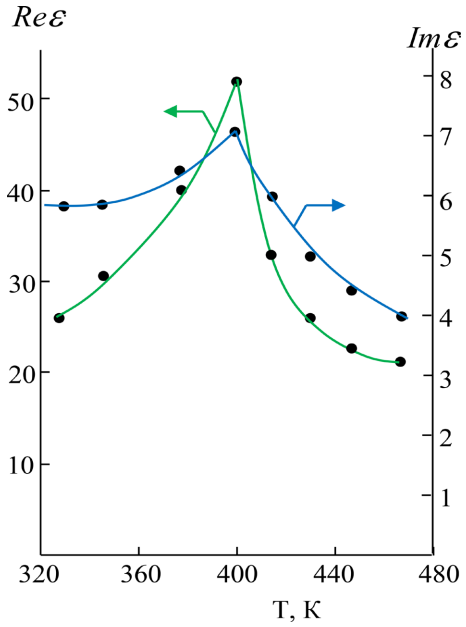

Figure 11. Dependence of the dielectric permittivity of $(Bi_{0.3}Sb_{0.7})_2Te_3$ on temperature.

the film matrix. The voltage distribution of microwave fields acquires a random value due to the inhomogeneity of the studied material. This is associated with the fact that, within each region of the film, components of the heterogeneous medium with different electrical and dielectric properties may exist. Fluctuations of the electric fields in spatially localized regions differ from zero. Under uniaxial deformation, acting on the film, re-distribution of localized carriers and changes in the concentration of free charge carriers occur. Consequently, the electronic contribution to the dielectric permittivity decreases and qualitatively corresponds to the experimental observations.

A pronounced value of the dielectric permittivity may result from the formation of heterogeneous structures during the vacuum deposition process of the films. In polycrystalline lead selenide films, the real component of the impedance is predominantly associated with the conductive regions, whereas the imaginary component corresponds to the insulating or non-conductive regions. This interpretation is supported by the effective medium theory, which adequately characterizes the electrical conductivity and dielectric permittivity of composite systems comprising both conductive and non-conductive phases, provided that the real part (Reσ) and the imaginary part (Imσ) differ by no more than an order of magnitude. Such a theoretical framework facilitates understanding the macroscopic electrical behavior of these complex materials by considering the interplay between microstructural heterogeneity and electrical response. It also allows for predictive modeling of the transport properties and dielectric response as a function of composition and microstructural parameters.

If the heterogeneous medium under study consists of two phases, then in the case of $\sigma_1 \gg \sigma_2$ the effective medium theory provides correct results not for all values of the volume fraction of the low-resistance component, but only starting

from those that correspond to the percolation threshold $\theta = \theta_c$ [19].

Due to the constant frequency, the relationship between the dielectric permittivity and electrical conductivity of $(Bi_{0.3}Sb_{0.7})_2Te_3$ films and the reciprocal temperature aligns with the findings reported in studies [22]-[25]. The experimental data demonstrate that by varying the volume fraction of inclusions, the system can approach the percolation threshold region.

5. Conclusions

The observed phenomena indicate a complex interplay of physical processes influencing the dielectric response of these materials $(Bi_{0.3}Sb_{0.7})_2Te_3$. Specifically, the sign inversion of the temperature coefficient of dielectric permittivity suggests the presence of competing polarization mechanisms within the solid solution matrix. The impedance extrema observed within at a frequency of $\omega = 5.1 \times 10^{10}$ Hz, the 350 - 450 K temperature interval further corroborate the involvement of multiple relaxation processes and interfacial effects at the grain boundaries.

These independent resonant mechanisms collectively govern the electrical behavior of the films, including the frequency matching between the applied alternating voltage and electron hopping dynamics, the temporal alignment of the measurement signal with the barrier layer formation time, and the resonance conditions between the external microwave field and structural constituents of the sample.

Such insights provide a foundation for tailoring the electrical and dielectric properties of $(Bi_{0.3}Sb_{0.7})_2Te_3$ solid solutions, enabling their integration into advanced microelectronic components, microwave devices, and precision measurement instruments in materials science. Future research may focus on optimizing these resonant conditions to enhance device performance and sensitivity.

Conflicts of Interest

The authors declare no conflicts of interest regarding the publication of this paper.

References

[1] Masood, K.B., Farooq, U. and Singh, J. (2020) Evolution of the Structural, Dielectric and Electrical Transport Properties of Bi_2Te_2 Nano-Sticks Synthesized via Polyol and Solvothermal Routes. *Physica B: Physics of Condensed Matter*, **588**, Article 412183. https://doi.org/10.1016/j.physb.2020.412183

[2] Dybov, V.A., Serikov, D.V., Fedorova, E.N., Sineckaya, D.A., Mozgovoy, P.S. and Dyaki, M.S. (2018) Structure and Mechanical Properties of Compacted Semiconductors Based on Bi_2Te_2-Sb_2Te_2 Solid Solutions Obtained by Hot Pressing and Subsequent Surface Treatments. *Bulletin of Voronezh State Technical University*, **18**, 191-197.

[3] Belonogov, E.K., Dybov, V.A., Kostyuchenko, A.V., Kushchev, S.B., Sanin, V.N., Serikov, D.V. and Soldatenko, S.A. (2017) Surface Modification of Thermoelectric Branches Based on Bi_2Te_2-Bi_2Se_2 Solid Solutions by Pulsed Photon Processing. *Condensed Media and Interphase Boundaries*, **19**, 479-488.

[4] Tasi, C., Tseng, Y., Jian, S., Liao, Y., Lin, C., Yang, P., *et al.* (2015) Nanomechanical

Properties of Bi_2Te_3 Thin Films by Nanoindentation. *Journal of Alloys and Compounds*, **619**, 834-838. https://doi.org/10.1016/j.jallcom.2014.09.028

[5] Wang, Z., Matsuoka, K., Araki, T., Akao, T., Onda, T. and Chen, Z. (2014) Extrusion Behavior and Thermoelectric Properties of $Bi_2Te_{2.85}Se_{0.15}$ Thermoelectric Materials. *Procedia Engineering*, **81**, 616-621. https://doi.org/10.1016/j.proeng.2014.10.049

[6] Abdullaev, N.A., Abdullaev, N.M., Aliguliyeva, H.V., Kerimova, A.M., Mustafayeva, K.M., Mamedova, I.T., *et al.* (2013) The Mechanism of Charge Transfer in $Bi_2(Te_{0.9}Se_{0.1})_3$ Solid Solution Thin Films. *Semiconductors*, **47**, 602-605. https://doi.org/10.1134/s1063782613050023

[7] Sulaymonov, K.M. (2017) The Effect of Cyclic Deformation on the AC Conductivity of $(Bi_{0.2}Sb_{0.7})_2Te_2$ Films. *Technical Physics Journal*, **87**, 471-472.

[8] Sulaymonov, H.M. and Yuldashev, N.K. (2016) Effect of Internal Stresses on the Static Strain Characteristics of P-$(Bi_{0.2}Sb_{0.7})_2Te_3$ Composite Films. *Journal of Surface Investigation. X-Ray, Synchrotron and Neutron Techniques*, **10**, 878-882. https://doi.org/10.1134/s1027451016040364

[9] Yuldashev, N.Kh. and Sulaymonov, Kh.M. (2021) Piezoresistivity of Crystals and Polycrystalline Films of Narrow-Bandgap Semiconductors Like PBS. Fergana Publishing House, 132 p.

[10] Sulaymonov, Kh.M. and Yuldashev, N.Kh. (2015) Strain-Resistive Properties of $(Bi_{0.25}Sb_{0.75})_2Te_2$ Films at One-Sided Cyclic Alternating Strains. T*he Third European Conference on Physics and Mathematics*, Vienna, 19 p.

[11] Gadzhiev, G.M., Gamzatov, A.G., Aliev, R.A., Abakarova, N.S., Emiraslanova, L.L., Markelova, M.N., *et al.* (2020) Temperature-Frequency Dependence of the Dielectric Response in $LuFe2O_4$ Multiferroics. *Physics of the Solid State*, **62**, 765-769. https://doi.org/10.1134/s1063783420050066

[12] Aliev, R.A., Gamzatov, A.G., Gadzhiev, G.M., Abakarova, N.S., Kaul', A.R., Markelova, M., *et al.* (2018) Effect of the Alternating Electric Field Frequency on the Temperature Spectra of Impedance in Ceramic Multiferroic $LuFe_2O_4$. *Physics of the Solid State*, **60**, 1073-1077. https://doi.org/10.1134/s1063783418060033

[13] Siddikov, R.U., Sulaymonov, K.M. and Yuldashev, N.K. (2025) Strain-Resistive Properties of $(Bi_{0.25}Sb_{0.75})_2Te_3$ Films at One-Sided Cyclic Alternating Strains. *East European Journal of Physics*, **1**, 190-196. https://doi.org/10.26565/2312-4334-2025-1-19

[14] Stepanov, N.P., Kalashnikov, A.A. and Ulashkevich, Y.V. (2010) Optical Functions of Bi_2Te_2-Sb_2Te_2 Solid Solutions in the Range of Plasmon Excitation and Interband Transitions. *Optics and Spectroscopy*, **109**, 893-898. https://doi.org/10.1134/s0030400x1012012x

[15] Lavrov, I.V. (2023) Methods for Calculating the Effective Electrophysical Properties of Heterogeneous Media Considering Various Structural Features: A Review. *Izvestiya Vysshikh Uchebnykh Zavedenii*, **28**, 403-430.

[16] Yurasov, A.N. and Yashin, M.M. (2018) The Effective Medium as a Tool for Analyzing the Optical Properties of Nanocomposites. *Russian Technological Journal*, **6**, 56-66.

[17] Bourgecis, P.C. and Maulin, M.V. (1967) Proportion Study of the Crystallographic and Physical Properties of PbTe Thin Films Evaporated in Vacuum on Amorphous or Oriented Substrates. *Comptes Rendus de l'Académie des Sciences*, **264**, 1830-1831.

[18] Zhou, J., Wang, Y., Sharp, J. and Yang, R. (2012) Optimal Thermoelectric Figure of Merit in Bi_2Te_2/Sb_2Te_2 Quantum Dot Nanocomposites. *Physical Review B*, **85**, 1-12. https://doi.org/10.1103/physrevb.85.115320

[19] Stepanov, N.P. and Kalashnikov, A.A. (2010) Features of Reflection Spectra of Single Crystals of Bi_2Te_2-Sb_2Te_2 Solid Solutions in the Region of Plasma Effects. *Semiconductors*, **44**, 1129-1133. https://doi.org/10.1134/s1063782610090034

[20] Zhang, Z., Sun, M., Liu, J., Cao, L., Su, M., Liao, Q., *et al.* (2022) Ultra-Fast Fabrication of Bi2te3 Based Thermoelectric Materials by Flash-Sintering at Room Temperature Combining with Spark Plasma Sintering. *Scientific Reports*, **12**, Article No. 10045. https://doi.org/10.1038/s41598-022-14405-5

[21] Stepanov, N.P., Gilfanov, A.K. and Trubitsyna, E.N. (2019) Correlation of the Optical and Magnetic Properties of Bi_2Te_2-Sb_2Te_2 Crystals. *Semiconductors*, **53**, 765-767. https://doi.org/10.1134/s1063782619060265

[22] Güçlü, Ç.Ş., Altındal, Ş., Ulusoy, M. and Tezcan, A.E. (2024) The Study of the Dependence of Dielectric Properties, Electric Modulus, and Ac Conductivity on the Frequency and Voltage in the Au/(CdTe:PVA)/n-Si (MPS) Structures. *Journal of Materials Science*: *Materials in Electronics*, **35**, Article No. 1225. https://doi.org/10.1007/s10854-024-12921-w

[23] Fu, J., Huang, J. and Bernard, F. (2021) Electronic Structure, Elastic and Optical Properties of Bi_2Te_3/Sb_2Te_3 Thermoelectric Composites in the Periodic-Superlattice Thin Films. *Composites Communications*, **28**, Article 100917. https://doi.org/10.1016/j.coco.2021.100917

[24] Daliev, K.S., Ahmedov, M.M. and Onarkulov, M.K. (2021) Influence of the Temperature and Cyclic Deformations of $(Bi_xSb_{1-x})_2Te_2$ Films on Their Resistance. *Journal of Engineering Physics and Thermophysics*, **94**, 1369-1373. https://doi.org/10.1007/s10891-021-02419-1

[25] Akhmedov, T., Otazhonov, S.M., Khalilov, M.M., Yunusov, N., Mamadzhanov, U. and Zhuraev, N.M. (2021) Effective Dielectric Permeability and Electrical Conductivity of Polycrystalline PbTe Films with Disturbed Stochiometry. *Journal of Physics*: *Conference Series*, **2131**, Article 052008. https://doi.org/10.1088/1742-6596/2131/5/052008